PAPER

Antibacterial activity of biogenic silver and gold nanoparticles synthesized from *Salvia africana-lutea* and *Sutherlandia frutescens*

IOP Publishing Nanotechnology

Nanotechnology **31** (2020) 505607 (15pp) https://doi.org/10.1088/1361-6528/abb6a8

Antibacterial activity of biogenic silver and gold nanoparticles synthesized from *Salvia africana-lutea* and *Sutherlandia frutescens*

Phumuzile Dube[1], Samantha Meyer[2], Abram Madiehe[1] and Mervin Meyer[1]

[1] DSI/Mintek Nanotechnology Innovation Centre Biolabels Node, Department of Biotechnology, University of the Western Cape, Cape Town, South Africa
[2] Department of Biomedical Sciences, Faculty of Health and Wellness Sciences, Cape Peninsula University of Technology, Cape Town, South Africa

E-mail: memeyer@uwc.ac.za

Received 14 June 2020, revised 2 September 2020
Accepted for publication 9 September 2020
Published 6 October 2020

Abstract

Nanoparticles (NPs) synthesized using various chemical and physical methods are often cytotoxic which restricts their use in biomedical applications. In contrast, metallic biogenic NPs synthesized using biological systems such as plant extracts are said to be safer and their production more cost effective. NPs synthesized from plants with known medicinal properties can potentially have similar bioactivities as these plants. It has been shown that *Salvia africana-lutea* (SAL) and *Sutherlandia frutescens* (SF) have antibacterial activities. This study used water extracts of SAL and SF to produce biogenic silver NPs (AgNPs) and gold NPs (AuNPs). The antibacterial activity of AgNPs and AuNPs was tested against two pathogens (*Staphylococcus epidermidis* and *P. aeruginosa*). NP synthesis was optimized by varying the synthesis conditions which include synthesis time and temperature, plant extract concentration, silver nitrate ($AgNO_3$) concentration and sodium tetrachloroaurate (III) dihydrate ($NaAuCl_4 \cdot 2H_2O$) concentration. The NPs were characterized using Ultraviolet-visible (UV–vis) spectroscopy, dynamic light scattering, high-resolution transmission electron microscopy (HR-TEM), and Fourier transform infrared (FT-IR) spectroscopy. SAL was able to synthesize both Ag (SAL AgNP) and Au (SAL AuNP) nanoparticles, whilst SF synthesized Ag (SF AgNP) nanoparticles only. The absorbance spectra revealed the characteristic surface plasmon resonance peak between 400–500 nm and 500–600 nm for AgNP and AuNP, respectively. HR-TEM displayed the presence of spherical and polygon shaped nanoparticles with varying sizes whilst the Energy Dispersive x-ray spectra and selected area diffraction pattern confirmed the successful synthesis of the AgNPs and AuNPs by displaying the characteristic crystalline nature, optical adsorption peaks and lattice fringes. FT-IR spectroscopy was employed to identify the functional groups involved in the NP synthesis. The microtitre plate method was employed to determine the minimum inhibitory concentration (MIC) of the NPs and the extracts. The water extracts and SAL AuNP did not have significant antibacterial activity, while SAL AgNP and SF AgNP displayed high antibacterial activity. In conclusion, the data generated suggests that SAL and SF could be used for the efficient synthesis of antibacterial biogenic nanoparticles.

Keywords: antibacterial, gold nanoparticles, silver nanoparticles, *Salvia africana-lutea*, *Sutherlandia frutescens*, synthesis

(Some figures may appear in colour only in the online journal)

1. Introduction

The scientific interest in the synthesis of colloidal/metallic nanoparticles (NPs) using biological molecules has recently gained momentum. This is due to the general perception that biogenic nanoparticles are safer and environmentally friendly in comparison to metallic nanoparticles synthesized using physical and chemical methods, which have been reported to be toxic, labour intensive and expensive. Additionally, the use of harmful chemicals in the synthesis has been shown to limit the biological use of the nanoparticles [1].

Of the currently utilised biological systems, plants are most favoured as they are readily available and contain a wide variety of phytochemicals that can potentially reduce metal ions [2, 3]. Silver, gold, copper, platinum and titanium metals are widely used for nanoparticle synthesis, with silver and gold being the most popular due to their unique biological and optical properties [3–5]. Numerous plants have been used in the synthesis of AgNPs and AuNPs including *Medicago sativa, Azadirachta indica, Aspalathus hispida, Asparagus ribicundus*, and *Dicerothamnus rhinocer* [6–10]. *Salvia africana-lutea* (SAL) and *Sutherlandia frutescens* (SF) are two indigenous South African plants with a long history of use in traditional medicine. SAL has been used in the treatment of skin and gastric disorders whilst SF is traditionally known for its anticancer activities [11–13]. Rosmarinic and carnosic acid, potent flavonoids associated with significant anti-inflammatory, anti-microbial and anti-oxidant properties, have been shown to be the most abundant chemical constituents of SAL extracts. It was also reported that the trimers and tetramers of the plant possess antioxidant, anti-cancer and antimicrobial activity [12, 14]. The documented high levels of the non-protein amino acid compound L-canavanine in SF, a compound associated with anti-cancer and antimicrobial activity could explain the traditional use of the plant in cancer treatment [15]. The complex interaction of different compounds within the plant such as Pinitol, γ-aminobutyric acid, flavonoids, triterpene glycosides and other compounds has further contributed significantly to the ethnopharmacological ability of SF [16, 17]. There are thus several compounds present in the extracts of these two plants that could be responsible for the antibacterial activity reported for extracts of these plants. AgNPs and AuNPs synthesised from these extracts could possibly also incorporate these compounds into the NPs.

Extracts of SAL and SF have been shown to have some antimicrobial activity. The antibacterial activity of acetone, ethanol and water extracts of SF was previously tested on *P. aeruginosa, S. aureus, E. coli* and *Enterococcus faecalis* [13]. The extracts were prepared from the leaves of the plant and the study found that the MIC for these extracts including the water extract was 10 mg ml^{-1}. A study by Nielsen *et al* tested the antimicrobial activity of methanol extracts of SAL against several bacterial and fungal strains [18]. While the reported MIC for *E. coli*, MRSA and *Microsporum audouinii* was 39.06 μg ml^{-1}, the MIC for six other microorganisms was above 100 μg ml^{-1}. Kamatou and colleagues reported MIC values of <1 mg ml^{-1} for SAL methanol: chloroform extracts prepared from the aerial parts of the plants [19]. Since these two plants have not been used previously to synthesize nanoparticles, this study investigated whether silver and gold nanoparticles can be produced from these extracts and whether these nanoparticles have antibacterial activity.

The successful synthesis of NPs by bio-reduction and characteristics of nanoparticles are affected by different factors including the concentrations of the reactants, synthesis temperature and time. It is therefore important to optimize these parameters in the nanoparticle synthesis reaction. Additionally, the differences in the chemical composition of medicinal plants may also affect the properties and yield of the synthesized nanoparticles, further justifying the need for the optimization of the synthesis procedure. In this study we report on the optimal conditions to synthesize AgNPs and AuNPs using water extracts of SAL and SF. We show that while the water extract have no significant antibacterial activity against the bacterial strains we used, SAL AgNPs and SF AgNPs displayed high antibacterial activity.

2. Materials and methods

2.1. Chemicals and apparatus

Müeller-Hinton agar, Müeller-Hinton broth, sodium tetrachloroaurate (III) dihydrate ($NaAuCl_4 \cdot 2H_2O$), silver nitrate ($AgNO_3$), yeast peptone broth (YPB) and Greiner bio-one 96 well flat bottom polystyrene microplates were acquired from Sigma-Aldrich (St. Louis, USA). Bovine serum albumin (BSA) was purchased from Miles Laboratories (Pittsburgh, PA, USA). Dulbecco's phosphate buffered saline (DPBS), Minimum Essential Medium Eagle-Alpha modification (MEM-α) and Roswell Park Memorial Institute medium (RPMI) were acquired from Thermo-Fischer scientific (Waltham, Massachusetts, USA).

2.2. Plant material

Fresh whole plants of SAL and SF were supplied by Harry Goemans Garden centre (Kommetjie Road, Sunnydale, Cape Town). The plants were grown from a reliable source of seed. They were harvested during autumn and were not flowering during harvest time.

2.3. Plant extraction

The leaves and stem of the plants were harvested, washed with distilled water and air dried in the shade for 2 weeks. After drying, the plant material was finely ground and extracted. Water extracts were prepared by adding 50 ml of boiling distilled water to 5 g of plant material. The decoction was left stirring for 24 h at 25 °C, after which it was filtered through glass wool to entrap residual plant material. The extract was then filtered using Whatman No.4 paper and further micro-filtered using 0.45 μm filter, and subsequently freeze dried (VirTis Genesis 25 ES Freeze drier, SP Scientific, Warminster, USA). The dried extract was weighed and stored at 4 °C in the dark for future use.

2.4. Optimization of conditions for the synthesis and screening of AgNPs and AuNPs

The optimization of synthesis was performed in Griener flat-bottom 96-well plates using methods described by Elbagory and colleagues for the synthesis of NPs [7]. The water extract (40 μl) of SAL and SF was added at decreasing concentrations (serial dilutions from 50 to 1.5625 mg ml^{-1}) to each well. To this 200 μl of $AgNO_3$ or $NaAuCl_4 \cdot 2H_2O$ was added for the synthesis of AgNPs and AuNPs, respectively, thus making a reaction mixture ratio of 1:5 (Plant extract: $AgNO_3$ or $NaAuCl_4 \cdot 2H_2O$). The AgNPs and AuNPs were synthesized using 1 mM and 3 mM of $AgNO_3$ and $NaAuCl_4 \cdot 2H_2O$, respectively at two temperatures, 25 and 70 °C. The $AgNO_3$ and $NaAuCl_4 \cdot 2H_2O$ were all preheated at the specific synthesis temperature prior to synthesis. The AgNPs were synthesized in the dark to prevent the photoactivation of $AgNO_3$. The synthesis took place over a 24 h period and the ultraviolet-visible (UV–vis) spectra of each sample was measured after 1, 3, 6 and 24 h using a POLARstar Omega spectrophotometer (BMG labtech, Germany). The synthesis of AgNPs and AuNPs was up-scaled to a final volume of 100 ml for further characterization, stability assays and application using the determined optimum synthesis conditions of plant extract concentration, $AgNO_3$ or $NaAuCl_4 \cdot 2H_2O$ concentration, temperature and time.

2.5. Characterization of synthesized AgNPs and AuNPs

The surface plasmon resonance (SPR) of the synthesized nanoparticles was measured by recording the UV–vis spectra ranging from 300 nm to 700 nm. Following up-scaled synthesis, the synthesized AgNPs and AuNPs were centrifuged at 13 000 rotations per minute (rpm) using the Eppendorf AG centrifuge 5417 R with a standard rotor (F-45-30-11) for 15 min and the pellets were washed three times with autoclaved distilled water as described previously [7]. This was performed to remove any residual phytochemicals and $AgNO_3$ or $NaAuCl_4 \cdot 2H_2O$ not utilised in the nanoparticle synthesis reaction. After each wash, the nanoparticles were re-suspended in volumes of water that was equal to total reaction volume. This was done to maintain the same nanoparticle concentration after washing the nanoparticles. In Eppendorf tubes, 1 ml of synthesized nanoparticles were centrifuged at 13 000 rotations per minute (rpm) for 15 min and the pellets air dried at 25 °C. The dried pellets were weighed and the quantity of synthesized nanoparticles was determined as the mass of dried pellet in 1 ml of synthesized nanoparticles. The hydrodynamic size, poly dispersity index (PDI) and zeta potential (ZP) of the synthesized nanoparticles were determined using the dynamic light scattering (DLS) technique. The analysis was performed using a Zetasizer Nano ZS90 (Malvern Instruments Ltd, UK) with a 90° scattering angle at 25 °C. The washed nanoparticles were diluted (1:10, v v^{-1}) and placed into either the polystyrene cuvette for hydrodynamic size and PDI determination or the Disposable Capillary Cell (DTS1070) cuvettes for ZP analysis.

2.5.1. High-resolution transmission electron microscopy (HR-TEM), energy dispersive x-ray spectra (EDX) and selected area diffraction pattern (SAED)

Synthesized, washed AgNPs and AuNPs were prepared by placing a single drop of sample solution onto a carbon-coated copper grid. These were allowed to dry for 10 min under a Xenon lamp, after which the grids were analysed under the transmission electron microscope (Field Emission Transmission Electron Microscope, Tecnai F20, FEI Company, Oregon USA) as described previously [7]. The microscope was operated at an acceleration voltage of 200 kV in a bright field mode. Concurrently, the Energy Dispersive x-ray spectra (EDX) were collected using a lithium doped silicon detector cooled using EDAX liquid nitrogen. Selected area diffraction pattern (SAED) was also determined to characterize the crystalline nature of the synthesized nanoparticles.

2.5.2. Fourier transform infrared (FT-IR) spectroscopy

FT-IR analysis was performed according to a previously reported method using the PerkinElmer spectrum one FT-IR spectrophotometer (Waltham, MA, USA) [20]. The purified dried nanoparticles were mixed with potassium bromide (KBr) and pressed into a pellet for analysis. Pressed pure KBr was used for background correction.

2.6. Stability analysis of synthesized AgNPs and AuNPs

In a 96-well plate, the washed nanoparticles (100 μl) were incubated with an volume of biological media as described previously [21]. The *in vitro* stability of synthesized AgNPs and AuNPs was tested by incubating the nanoparticles with biological media (Minimum Essential MEM-α, MHB, Roswell Park Memorial Institute medium, YPB), BSA, and DPBS. The stability of the synthesized AgNPs and AuNPs was determined by observing the changes in the UV–vis spectra (POLARstar Omega spectrophotometer, BMG labtech, Germany) after 0, 1, 12 and 24 h incubation at 37 °C in the respective media or buffer.

2.7. Antibacterial testing

2.7.1. Bacterial strains

Staphylococcus epidermidis (*S. epidermidis*, ATCC 12 228) and *P. aeruginosa* (*P. aeruginosa*, ATCC 27 853) was acquired from American Type Culture Collection (ATCC, Manassas, VA, USA) and used as representative bacterial strains for the antibacterial testing.

2.7.2. Determining the minimum inhibitory concentration (MIC)

Microbial cultures were prepared by inoculating MHB with single bacterial colonies and incubating the inoculum overnight at 37 °C in a horizontal type-shaking incubator (LM-530D, Taiwan). The bacterial suspensions were standardized to 0.5 McFarland ($\sim$1.5 x 10^8 cells ml^{-1}) at spectrophotometric wavelength of 630 nm and further diluted to a final concentration of 5 $\times$ 10^5 cells ml^{-1}. The diluted bacterial cultures were treated with the water extracts and NPs. Treatments with the water extracts were performed at concentrations ranging between 50 and 0.39 mg ml^{-1}, while the concentrations

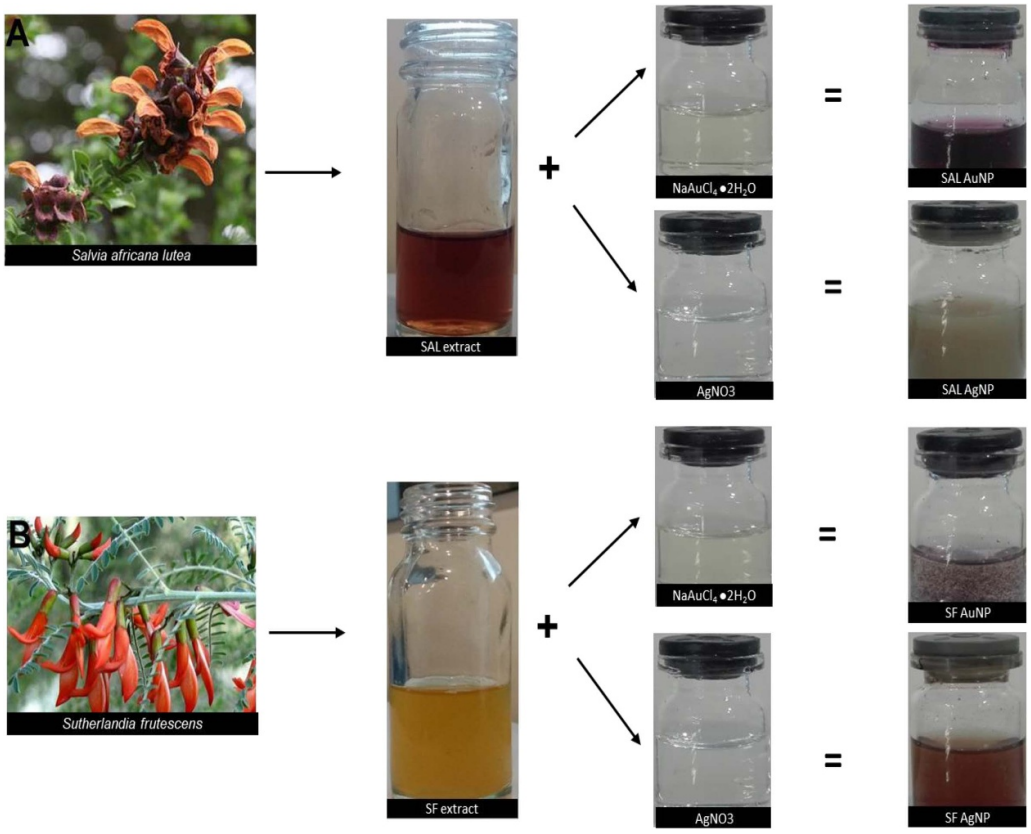

Figure 1. Illustration of synthesis of AgNPS and AuNPs from SAL, and SF. (A) represents biogenic nanoparticle synthesis using SAL extract and (B)using SF extract.

of the NPs ranged from 1.5 to 0.012 mg ml^{-1}. Ampicillin was used as a positive control. Minimum Inhibitory Concentration (MIC) was determined as described by Balouiri *et al* [22]. The lowest concentration that inhibited visible bacterial growth was recorded as the MIC. The experiment was done in triplicate.

2.8. Statistical analysis

The data are expressed as mean ± standard deviation (SD). Statistical differences between the means were considered significant at $p < 0.05$ according to two-way ANOVA test followed by a post hoc multiple comparison analysis (Turkey"s test) using the GraphPad^{TM} PRISM6 software package.

3. Results

3.1. Establishing the optimum conditions for the synthesis of AgNPs and AuNPs

The synthesis of AgNPs and AuNPs from both SAL and SF was optimized by varying reaction temperature, reaction time, plant extract concentration and $AgNO_3$ or $NaAuCl_4 \cdot 2H_2O$ concentration. The first indication of successful biosynthesis of nanoparticles was a uniform colour change as illustrated in figure 1. AgNP synthesis produced a brown solution for both SAL and SF. AuNP synthesis with SAL produced a red-violet solution, while AuNP synthesis with SF produced a clear solution with visible particulates.

3.1.1. Determining the optimum concentration (OC) of reactants for the synthesis of AgNPs and AuNPs It has been documented that both 1 mM and 3 mM of $AgNO_3$ and $NaAuCl_4 \cdot 2H_2O$ are commonly used for AgNP and AuNP synthesis, respectively [23–25]. These concentrations of $AgNO_3$ and $NaAuCl_4 \cdot 2H_2O$ were thus used in this study. For SAL and SF plant extracts, the colour changes were more rapid and homogenous when synthesis was performed with 3 mM $AgNO_3$, while similar synthesis reactions could only be observed with SAL plant extracts and 1 mM $NaAuCl_4 \cdot 2H_2O$. Hence, 1 mM $NaAuCl_4 \cdot 2H_2O$ was selected for the synthesis of SAL AuNPs and 3 mM $AgNO_3$ as the optimum concentration for SAL AgNPs and SF AgNPs. With respect to plant extract concentrations, the plant extract concentrations used were 50, 25, 12.5, 6.25, 3.125 and 1.5625 mg ml^{-1}. The reactions were monitored for colour changes at different time intervals for 24 h. SF extracts were observed to produce a brown solution at 6.25 and 3.125 mg ml^{-1} with $AgNO_3$, while SAL extracts produced a brown solution with $AgNO_3$ and violet-red with $NaAuCl_4 \cdot 2H_2O$ at concentrations of 3.125 mg ml^{-1} and 1.5625 mg ml^{-1}. The UV–vis spectrum was recorded at specific time points as shown in figure 2. The screen for AgNP synthesis showed absorbance peaks for SAL and SF with 3 mM $AgNO_3$, while the screen for AuNP synthesis showed

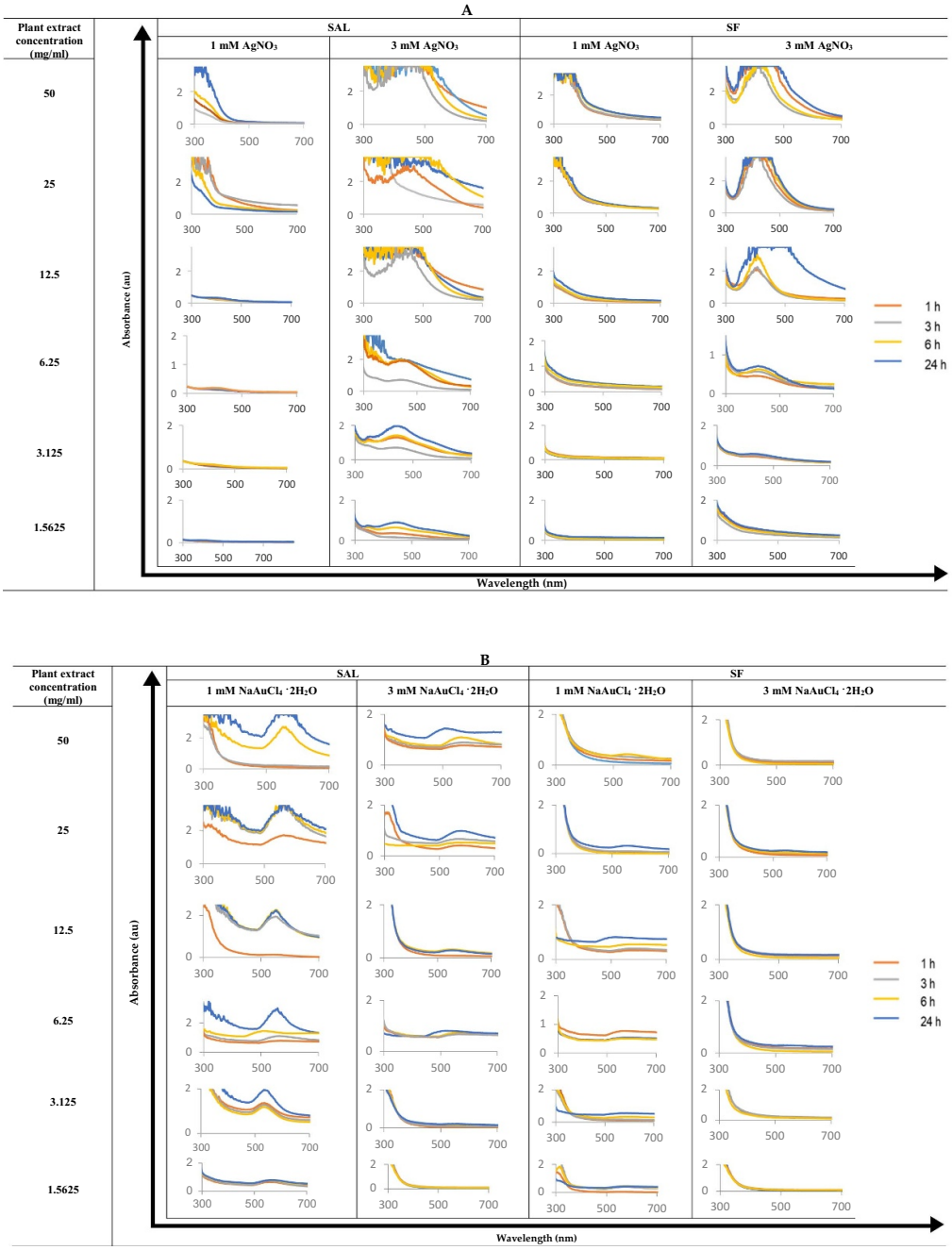

Figure 2. Effects of reaction time, plant extract concentration and $AgNO_3$ or $NaAuCl_4 \cdot 2H_2O$ concentration on UV–vis spectra of synthesised nanoparticles at 70 °C. (A) shows the UV–vis spectra for synthesis of AgNP and (B) shows the spectra for AuNP synthesis.

absorbance peaks for SAL with 1 mM $NaAuCl_4 \cdot 2H_2O$, but not SF. For both AgNPs and AuNPs, increased plant extract concentration (12.5, 25 and 50 mg ml^{-1}) resulted in increased absorbance intensity. Hence 6.25 mg ml^{-1} of SF plant extract was selected for SF AgNP synthesis and 3.125 mg ml^{-1} of SAL plant extract was selected for the optimum synthesis of SAL AgNP and SAL AuNP.

3.1.2. Determining the optimum reaction temperature for AuNP and AgNP synthesis The AgNPs and AuNPs were synthesized over a 24 h period at both 25 °C (data not shown) and 70 °C (figure 2), however, no colour changes were observed for all reactions at 25 °C. Furthermore, absence of absorbance peaks on the UV–vis spectra, similar to those observed at 70 °C for SF AuNPs shown in figure 2, was recorded for all nanoparticle synthesis at 25 °C. Hence, 70 °C was selected as the optimum temperature for SAL AgNP, SAL AuNP and SF AgNP synthesis due to the presence of absorbance peaks characteristic of AgNPs and AuNPs.

3.1.3. Determining the optimum reaction time for AuNP and AgNP synthesis The UV–vis absorbance spectra were measured after 1, 3, 6 and 24 h. As the synthesis progressed the

Table 1. Summary of optimum conditions of AgNP and AuNP synthesis using SAL and SF plant extract.

Plant name	Metal ion	Nanoparticle abbreviation	Optimum plant extract concentration (mg ml^{-1})	Optimum $NaAuCl_4 \cdot 2H_2O$ or $AgNO_3$ concentration (mM)	Optimum synthesis temperature (^oC)	Optimum synthesis time (h)
Salvia africana-lutea	Silver	SAL AgNP	3.125	3	70	24
Salvia africana-lutea	Gold	SAL AuNP	3.125	1	70	24
Sutherlandia frutescens	Silver	SF AgNP	6.25	3	70	24

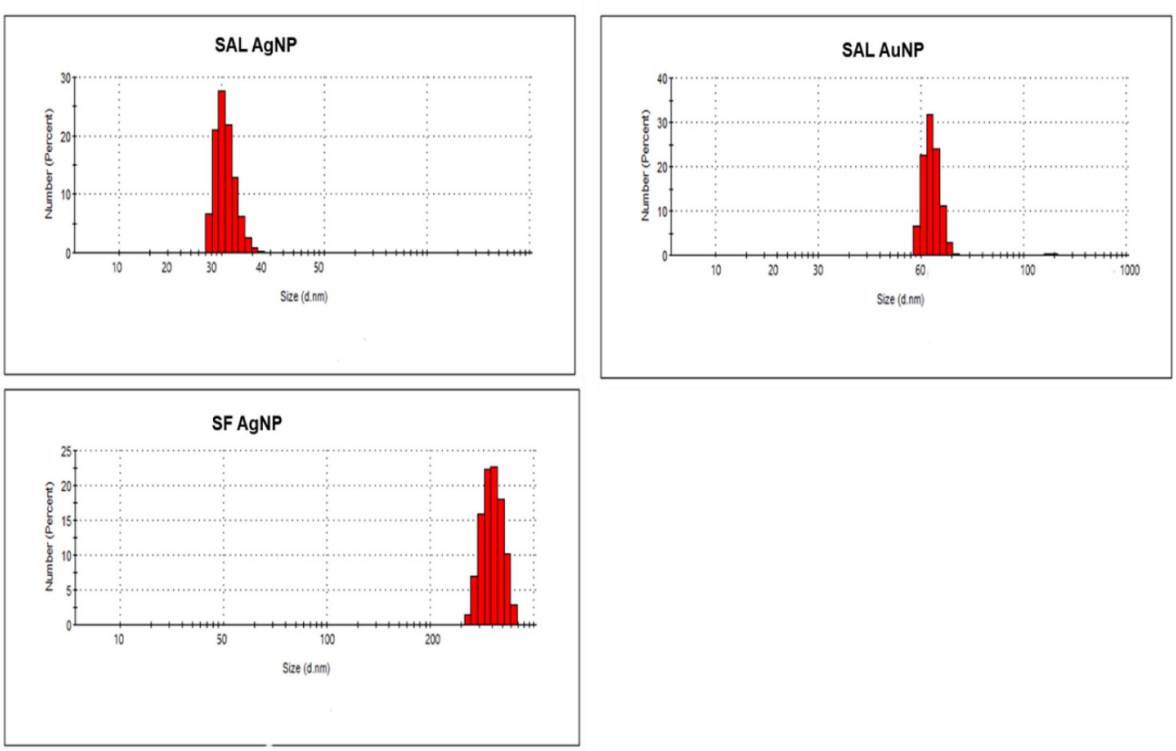

Figure 3. Size distribution by number of synthesized SAL AgNP, SAL AuNP and SF AgNP.

intensity of the absorbance peaks increased. Absorbance maxima from 400 to 500 nm and 500 to 600 nm were observed for SAL and SF AgNP (figure 2(A)) and SF AuNP (figure 2(B)), respectively. Based on the UV–vis absorbance spectra data at different temperatures, reaction times, plant extract concentration and $AgNO_3$ or $NaAuCl_4 \cdot 2H_2O$ concentrations the optimum synthesis conditions were determined and are summarised in table 1.

3.2. Characterization of the synthesized AgNPs and AuNPs by dynamic light scattering

DLS is a technique commonly used in the determination of particle size in colloidal suspensions [26]. The concentration of the colloidal suspensions was 1 mg ml^{-1}. DLS was used to determine three important characteristics of the synthesized AgNPs and AuNPs. These are hydrodynamic size (figure 3), PDI and ZP, which can be used to predict the behaviour of nanoparticles in biological media. The surface charge of colloidal nanoparticles was determined by measuring the ZP of the nanoparticles (figure 4). Table 2 shows the charge, size and distribution of the synthesized nanoparticles. All the synthesized nanoparticles displayed a PDI greater than 0.2 and ZP less than −30 mV.

3.3. Characterization of the synthesized AgNPs and AuNPs using high-resolution transmission electron microscopy (HR-TEM)

High-resolution transmission electron microscopy (HR-TEM) was employed to analyse the morphology and size of the synthesized nanoparticles. The synthesized Ag and Au nanostructures were polymorphic with varying sizes. This size variation was more pronounced with SAL AgNPs and SF AgNPs, as seen in figure 5. Although the predominating shape was spherical, SAL was also observed to produce polygon shaped AgNPs and AuNPs.

Size distribution curves for the synthesized nanoparticles measured from the HR-TEM images are indicated in figure 6. The highest frequency of SAL AgNPs and SAL AuNPs were

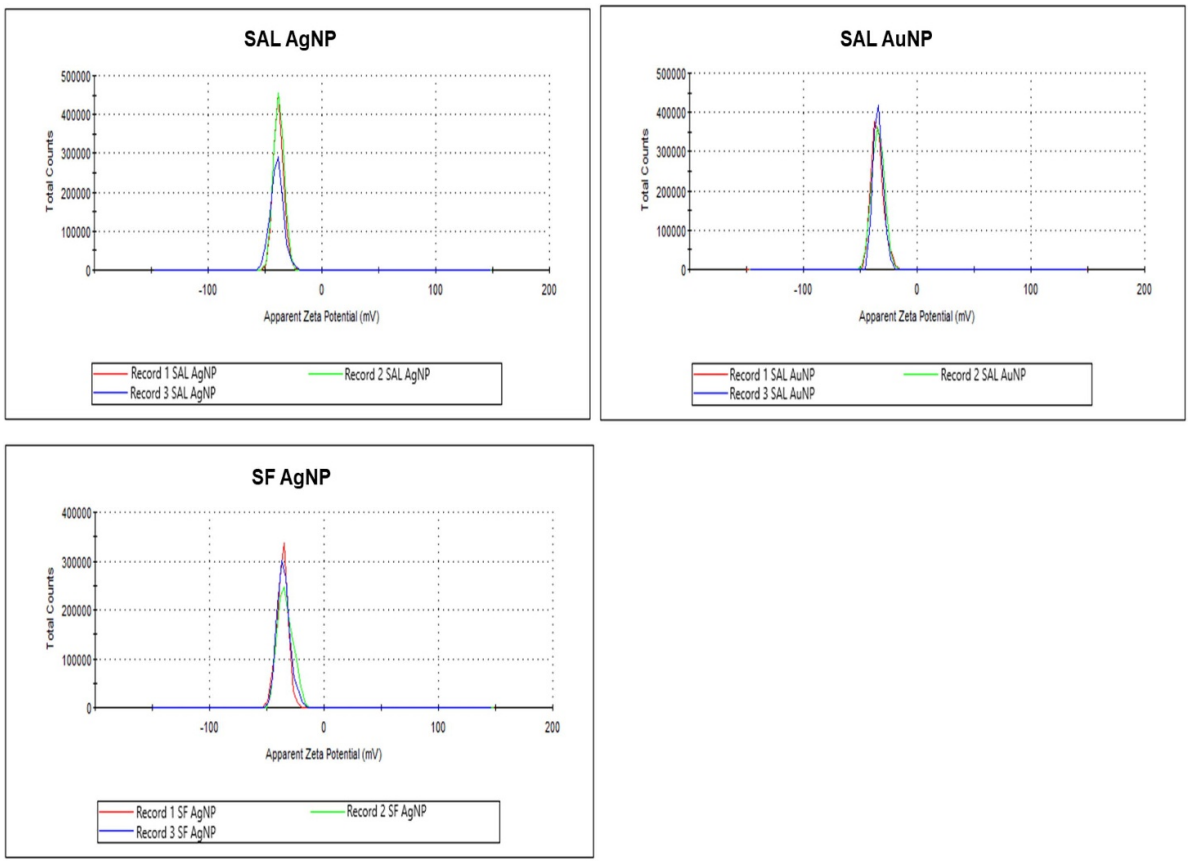

Figure 4. Zeta potential distribution curves of synthesized SAL AgNP, SAL AuNP and SF AgNP.

Table 2. Average hydrodynamic size, PDI and ZP of the AgNPs and AuNPs synthesized using the optimum conditions.

Nanoparticle	Average hydrodynamic size ± SD (nm)	Average PDI ± SD	Average ZP ± SD (mV)
SAL AgNP	34.63 ± 4.53	0.63 ± 0.03	−41.1 ± 2.00
SAL AuNP	63.27 ± 8.94	0.51 ± 0.03	−34.7 ± 1.39
SF AgNP	261.2 ± 10.40	0.612 ± 0.02	−35.7 ± 1.53

ranging from 6–8 nm to 10–15 nm, respectively, whilst the highest frequency of SF AgNPs was between 15 and 20 nm. The nanoparticle diameter as determined by HR-TEM is summarised in table 3.

Gold and silver elements were detected using EDX analysis in AuNP and AgNP, respectively as shown in figure 7. The position of strong optical adsorption peaks for Au was observed at 2.3, 9.7 and 11.3 keV and for Ag between 2.5 and 4 keV. The presence of nickel, copper, carbon, argon, oxygen and chlorine peaks were also found.

The crystalline nature of the synthesized AuNPs and AgNPs was observed as the lattice fringes with specific spacing, as illustrated in figure 8. The SAL AgNPs and SF AgNPs had a fringe spacing of 0.228 and 0.226 nm respectively, whilst the SAL AuNPs had 0.233 nm fringe spacing. The SAED patterns, which show the crystalline nature of the AgNPs and AuNPs, are also displayed. After indexing, the rings for SAL AuNPs were found to correspond with the (111), (200), (220) and (311) face-centered cubic (fcc) of gold whilst those for SAL AgNPs and SF AgNPs concur with (111), (200), (220), (222) and (311) fcc of silver [7].

3.4. Characterization of the synthesized AuNPs and AgNPs by Fourier transform infrared (FT-IR) spectroscopy

FT-IR measurements were done to identify the functional groups of phytochemicals present in SAL and SF extracts responsible for the reduction and/or stabilization of the synthesized AuNPs and AgNPs. The Infrared (IR) spectrum of SAL AgNPs displayed intense bands at 3414.29, 3241.07, 2920.96, 2049.04, 1625.92, 1237.48, 618.97 and 480.39 cm-1, whereas intense bands for SAL AuNPs were observed at 3706, 3563.05, 3405.97, 3236.06, 2907.03, 2045.03, 1618.43, 1257.18, 855.96 and 620.75 cm-1. In the IR spectrum of SF AgNPs, prominent absorption bands were located at 3551.94, 3411.17, 3238.56, 2911.52, 2053.49, 1625.97, 1259.13, 1041.76, 620.31 and 481.75 cm-1 (figure 9). The biosynthesized nanoparticles and the corresponding plant extracts used to synthesise the nanoparticles showed some similar

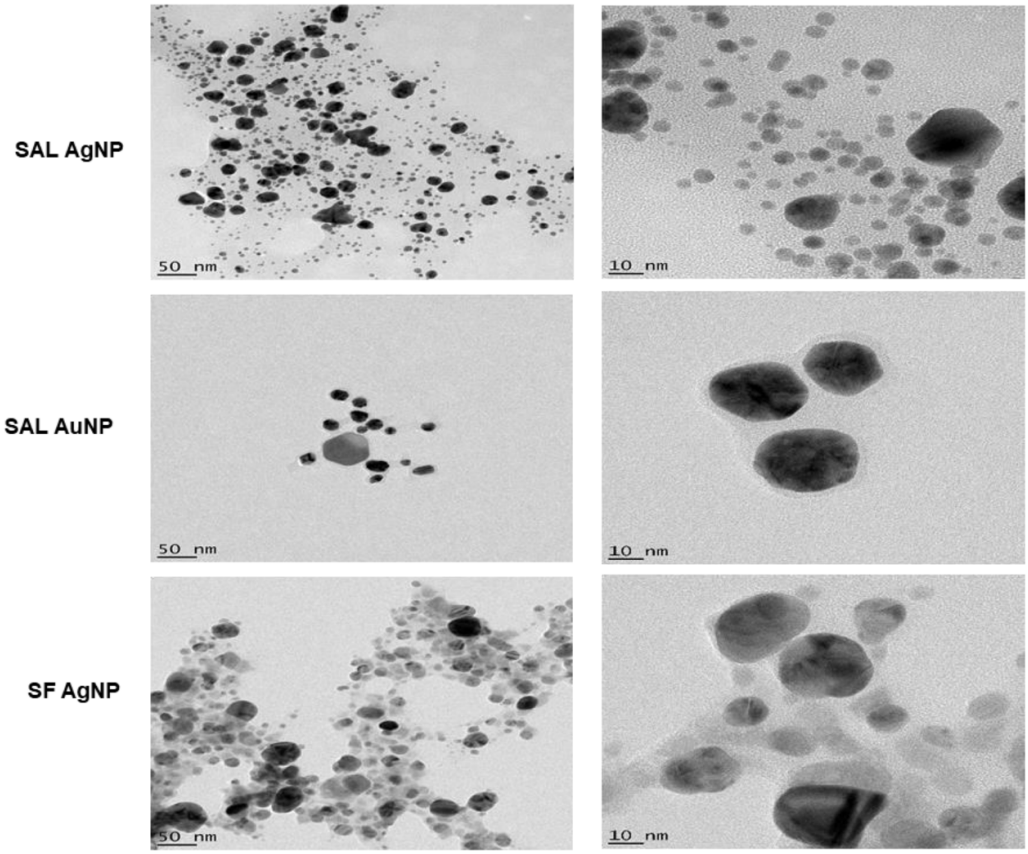

Figure 5. High Resolution Transmission Electron Microscopy (HR-TEM) images of the nanoparticles.

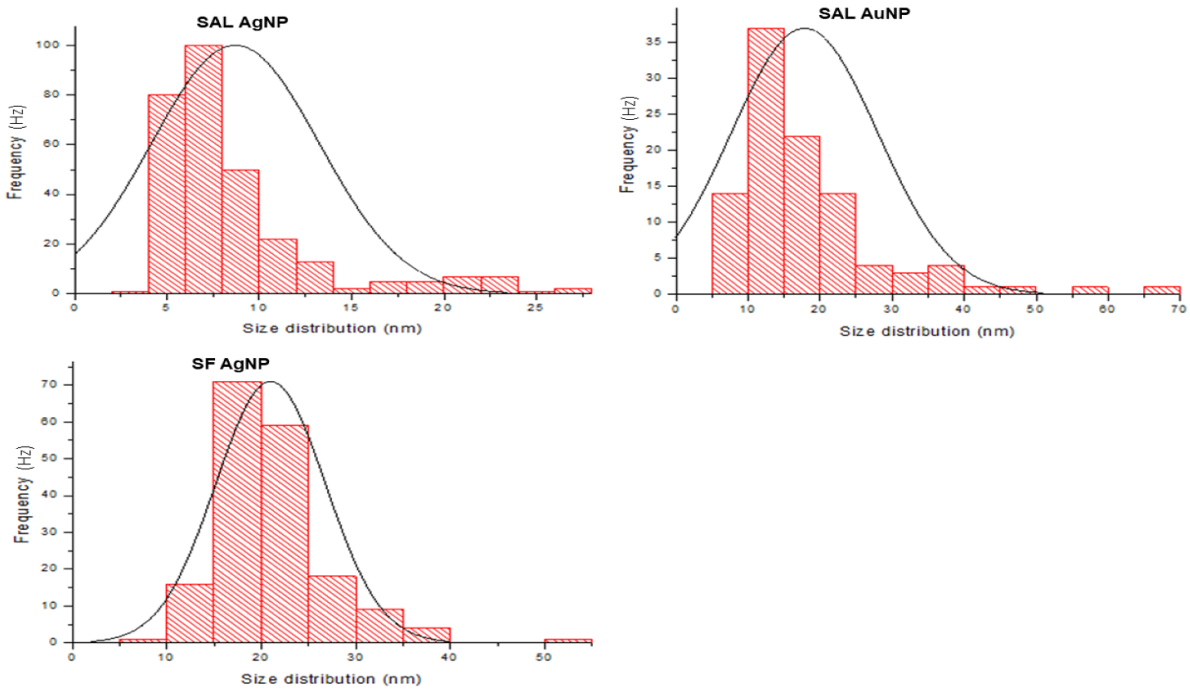

Figure 6. Size distribution curves for synthesized AgNPs and AuNPs as determined by HR-TEM.

bands, whilst some of the bands of the nanoparticles appeared shifted when compared to the FT-IR spectra of the extracts. Similar bands were observed in all the synthesized nanoparticles. The band shifts are summarised in table 4.

Table 3. Average particle diameter (PD) of synthesized nanoparticles.

Nanoparticle	Average PD ± SD (nm)
SAL AgNP	8.71 ± 5.13
SAL AuNP	17.84 ± 10.17

3.5. Stability of synthesized AgNPs and AuNPs in biological media

The stability of synthesized nanoparticles in solvents is an important parameter for their potential application. Stable nanoparticles are notably evenly distributed and do not agglomerate or aggregate when placed in a solvent. Changes in the UV–vis spectra of nanoparticles over time in the presence of a solvent can be used as an indication of nanoparticle stability. In this study, the stability of the synthesized nanoparticles was determined by evaluating changes in the UV–vis spectra over a period of 24 h as shown in figure 10. The UV–vis changes were observed after 0, 1, 12 and 24 h incubation of the synthesized nanoparticles in MEM-α, RPMI, BSA, DPBS, YPB and MHB. The synthesized nanoparticles and media were incubated at 37 °C. This temperature was selected since most of the intended biological applications of the nanoparticles was going to be performed at 37 °C in these media. The synthesized AgNPs and AuNPs were moderately stable, depicted by the minimal changes in the UV–vis spectra.

3.6. Antibacterial effects of SAL and SF water extracts and respective NPs

The MIC values for the water extracts were higher than 50 mg ml^{-1} as reported in table 5. SAL AgNPs, on the other hand, exhibited high antibacterial activity against *S. epidermidis* and *P. aeruginosa* with MIC values of 0.1875 and 0.375 mg ml^{-1} respectively. The growth of both bacterial strains were not affected by SAL AuNPs at the concentrations used in this study.

4. Discussion

4.1. Synthesis of AgNPs and AuNPs

The biosynthesis of NPs using plants involves the reduction of metallic ions by phytochemicals that are present in the plant extract. The reduction of the metallic ions is followed by nucleation and subsequent NP formation and may end with the capping of the NP with capping agents that stabilize the synthesised NPs [23]. The successful synthesis of AgNPs and AuNPs was indicated by the appearance of colour change after $AgNO_3$ or $NaAuCl_4 \cdot 2H_2O$ was incubated with the optimum concentration of the plant extract. The synthesized AgNP solution exhibited the characteristic brown colour whilst the AuNP solution appeared red-violet (figure 1). The synthesis of AuNPs using SF, failed to produce a uniform colour change and suggest that SF might require synthesis conditions other than the conditions e investigated in this study. The uniform colour change is a result of SPR of the synthesized nanoparticles [6]. The UV–vis spectra confirmed the synthesis of nanoparticles by displaying peaks characteristic of solutions of AgNPs and AuNPs. The intensity of the absorbance peak (λ-max) is reflective of the size and concentration of synthesized nanoparticles [27]. The SPR produced λ-max between 400 and 500 nm for AgNPs, and between 500 and 600 nm for AuNPs. These optical characteristics are a result of the excitation of the longitudinal plasmon vibration [28, 29]. The absence of a homogenous colour change and characteristic absorbance peak has been associated with the failure of nanoparticle synthesis [30], as observed when SF was reacted with $NaAuCl_4 \cdot 2H_2O$. The λ-max of SAL AgNP and SAL AuNP were around 472 and 532 nm, respectively, whereas for SF AgNP was around 432 nm, confirming nanoparticle synthesis.

4.2. Optimization of different synthesis parameters

The analysis of the morphology and size of synthesized nanoparticles is of great importance because the variation in size and shape of biogenic nanoparticles may affect their biomedical application. This variation is due to the uniqueness of the phytochemical blueprint of the plants. Additionally, several parameters of synthesis, which include reaction time, temperature and concentrations of the reactants, may affect the quality and quantity of the nanoparticles [7]. Numerous studies have used varying concentrations of $AgNO_3$ and $NaAuCl_4 \cdot 2H_2O$ in nanoparticle synthesis [7, 31–33]. However, 3 mM $AgNO_3$ and 1 mM of $NaAuCl_4 \cdot 2H_2O$ have consistently shown to be suitable concentrations for biogenic nanoparticle synthesis. This was corroborated by the observations of this study, which reported a more defined colour change when SAL AgNP, SAL AuNP and SF AgNP were synthesized.

Different concentrations of SAL and SF extracts (50, 25, 12.5, 6.25, 3.125 and 1.5625 mg ml^{-1}) were reacted with $AgNO_3$ and $NaAuCl_4 \cdot 2H_2O$ (3 mM and 1 mM) to produce Ag and Au nanoparticles, respectively. All the higher extract concentrations assessed (50, 25 and 12.5 mg ml^{-1}) showed colour change suggesting successful nanoparticle synthesis. In contrast, no colour changes were observed for SF extracts reacted with $NaAuCl_4 \cdot 2H_2O$ suggesting that AuNP was not produced. However, the absorbance peaks produced at higher plant concentrations were noisy which may suggest that high plant extract concentrations contain concentrated phytochemical content utilised in the synthesis. Furthermore, at lower plant extract concentrations, 6.25 mg ml^{-1} for SF extract with $AgNO_3$, and 3.125 mg ml^{-1} for SAL extract with $AgNO_3$ and $NaAuCl_4 \cdot 2H_2O$ displayed more defined absorbance peaks. Broader peaks were observed when 1.5625 mg ml^{-1} SAL extract was used to synthesise SAL AgNP and SAL AuNP, and 3.125 mg ml^{-1} SF extract in the synthesis of SF AgNP. Broader peaks result from the insufficiency of biomolecules required for capping and stabilization of the synthesized nanoparticles [30]. The variations in the values of absorbance signify changes in the nanoparticle size and concentration [34]. Sharper absorbance peaks observed for SAL AgNP and SAL

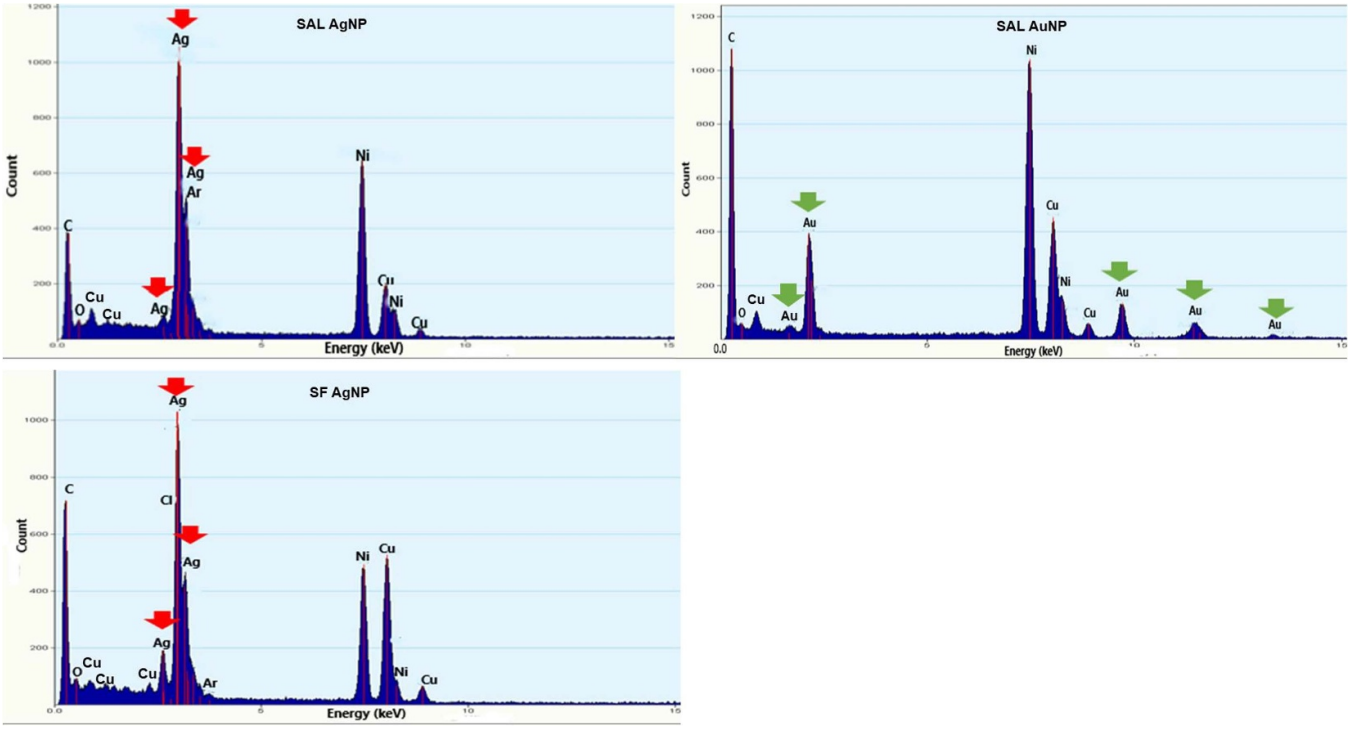

Figure 7. Energy Dispersive x-ray Spectroscopy (EDX) spectra of SAL AgNPs, SAL AuNPs and SF AgNPs. The red arrows show Ag and green arrows Au peaks.

AuNP corresponded with the generally smaller sized nanoparticles, while broader absorbance peaks were observed for larger sized SF AgNP. This observation was in agreement with observations reported by Ibrahim (2015) [35].

The reaction time was optimized by monitoring the reaction over a 24 h period. Interestingly, for all nanoparticles the intensity of the λ-max absorbance peaks increased with time, indicating an increase in the quantity of nanoparticles produced over time. Elbagory and colleagues reported on the correlation of the absorbance and number of nanoparticles in solution [7]. As the reaction temperature was increased, the synthesis rate of both AgNPs and AuNPs also increased. Hence, the synthesis temperature of 70 °C allowed for the successful synthesis of SAL AgNP, SAL AuNP and SF AgNP. Increase in synthesis temperature was previously shown to increase both the synthesis rate and final conversion of metallic ions to nanoparticles [27, 36].

4.3. Characterization of synthesized nanoparticles

4.3.1. The characterization of synthesized nanoparticles by hydrodynamic size, zeta potential and PDI. The average hydrodynamic size, ZP and PDI of the synthesized nanoparticles were determined using DLS and is reported in table 2. Hydrodynamic size is depended on the interaction of nanoparticles with the solvent the nanoparticles are suspended in. The average hydrodynamic size was 34.63, 63.27 and 261.20 nm for SAL AgNP, SAL AuNP and SF AgNP, respectively. All synthesized nanoparticles had an average ZP less than −30 mV (table 2). It is been suggested that nanoparticles with such high negative ZP values are stable [37]. This stability is a result of the strong repulsion forces existing between the negatively charged nanoparticles, preventing their aggregation. The PDI measures the distribution of nanoparticles in colloid suspension and is measured as a value between 0 and 1. A PDI value between 0.1 and 0.2 suggests that nanoparticles are monodispersed, *i.e.* the nanoparticles have a similar size and shape [38]. Considering the synthesized nanoparticles had PDI values greater than 0.2, the nanoparticles can be classified as polydispersed, *i.e.* of different size and shape.

4.3.2. High-resolution transmission electron microscopy (HR-TEM) As seen in figure 5, the HR-TEM revealed the presence of nanoparticles with different sizes and shapes. This corroborated the conclusion made from the PDI values reported in table 1. The hydrodynamic size of the synthesized nanoparticles was 34.63, 63.27 and 261.20 nm, whilst the HR-TEM core size was 8.71, 17.84 and 21 nm for SAL AgNP, SAL AuNP and SF AgNP, respectively. Such apparent discrepancies between size determination done by HR-TEM and DLS has been reported previously [7]. The hydrodynamic size is typically larger than the HR-TEM derived size as it is influenced by the interaction of the nanoparticle surface with the solvent [21]. Based on these results, our observations concurred with previously reported studies. The geometrical and size variation has been widely reported for biogenic nanoparticles and has been associated with the phytochemical profile of the selected plants [7, 39–41]. The common phytochemical groups responsible for the reduction of Ag and Au ions in

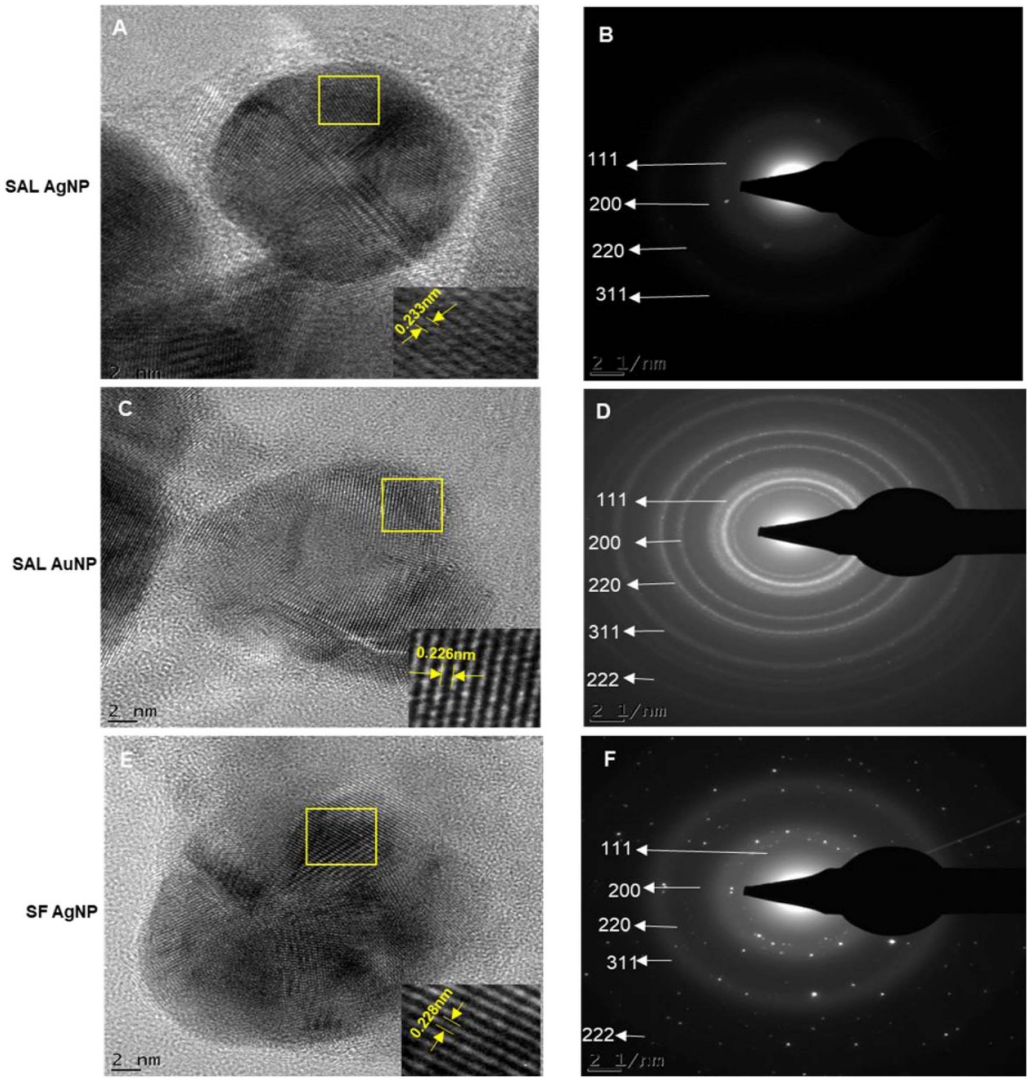

Figure 8. HR-TEM images and SAED analysis of the nanoparticles. (A), (C) and E show HR-TEM and lattice fringes. The inserts on (A), (C) and (E) shows the measurement of the lattice fringes for the respective nanoparticle. (B), (D) and (F) show the SAED.

the synthesis of nanoparticles have been identified as flavonoids, alkaloids, flavones, amino acids, steroids, polyphenols and proteins [29].

The elemental profile of the nanoparticles is shown on the EDX spectra (figure 7). The presence of strong optical adsorption peaks corresponding to Ag (2.5–4 keV) on the spectra for SAL AgNP and SF AgNP, and Au (2.3, 9.7 and 11.3 keV) for SAL AuNP further confirms the successful synthesis of the Ag and Au nanoparticles. Additionally, adsorption peaks corresponding to nickel, copper, carbon, argon, oxygen and chlorine elements were also observed. These elements could originate from the grid utilised during HR-TEM as well as plant extracts involved in the nanoparticle synthesis. The lattice fringes present on the synthesized nanoparticles confirm the crystalline nature of the nanoparticles (figure 8). This was further confirmed by the observed SAED pattern. The lattice fringe spacing was similar to that previously reported for AgNPs or AuNPs synthesized from *Murraya koenigii* [30], *Iresine herbstii* [39], *Pulicaria glutinosa* [20] and *Medicago sativa* [8]. Ring positioning for the synthesized AuNPs (111, 200, 220, 311 and 222 fcc) and AgNPs (111, 200, 220 and 311 fcc) on the SAED concurs with numerous published studies [7, 40–42].

4.3.3. Fourier transform infrared (FT-IR) spectroscopy FT-IR spectroscopy was performed on the extracts and nanoparticles to identify functional groups that are similar between the extract and the nanoparticles. The Infrared (IR) spectroscopy observes the vibrations of molecular bonds and hence provides information on the nature of the bonds and functional groups in the molecules. The generated information can be utilised to identify functional groups from phytochemicals that are involved in the bioreduction of $AgNO_3$ and $NaAuCl_4 \cdot 2H_2O$ and thus confirm the involvement of the phytochemicals in the synthesis of the nanoparticles. Numerous studies suggest that different phytochemicals may play a role in the synthesis of biogenic AgNP and AuNP [21, 29, 30]. Figure 9 shows the presence of several functional groups that are present in both the extract and nanoparticles. The

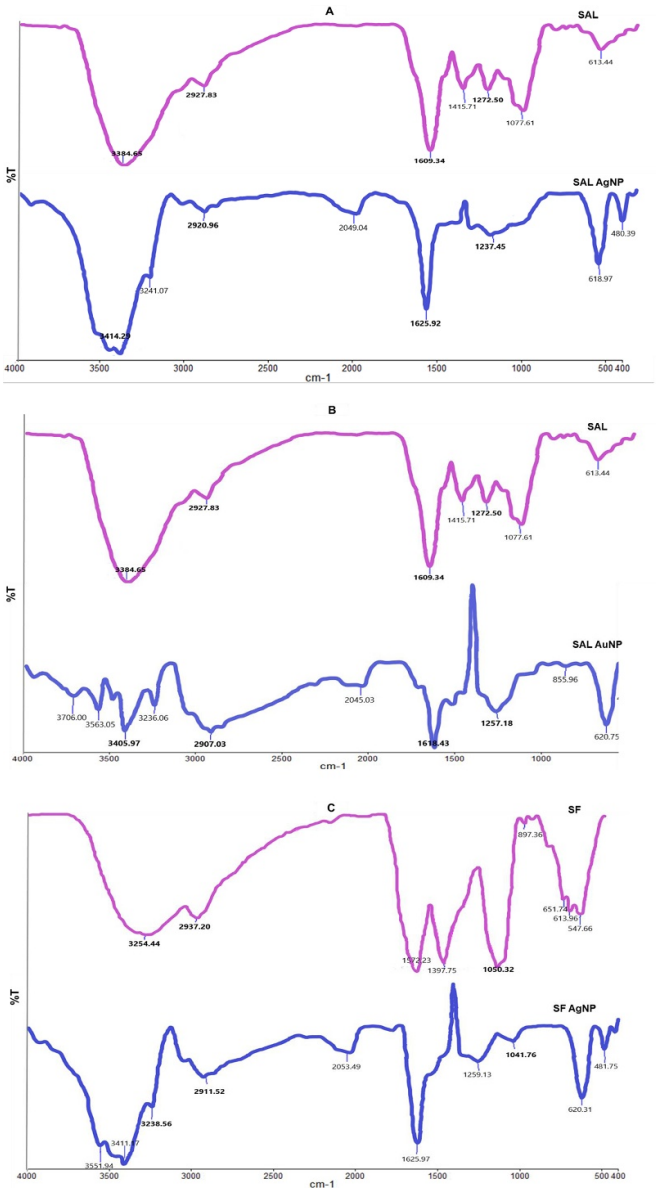

Figure 9. FT-IR spectra of plant extracts and the respective nanoparticles synthesized from the extracts. (A)shows the FT-IR spectra of SAL and SAL AgNP, (B) shows the FT-IR spectra of SAL and SAL AuNP and (C) shows the FT-IR of SF and SF AgNP.

spectra of some functional groups appear to be shifted in the nanoparticle samples. The shifts are summarised in table 4 and suggest the involvement of the corresponding functional groups in the synthesis of the nanoparticles. Interestingly, similar peaks were observed in the FT-IR spectra of synthesized nanoparticles from both plants, suggesting similar functional groups and therefore similar phytochemicals may be involved in the synthesis of the nanoparticles. For instance visible bands at 2920.96, 2907.03 and 2911.52 cm-1 may be a result of the C-H stretch alkanes whilst the defined bands at 3414.29, 3405.97 and 3411.17 cm-1 for SAL AgNP, SAL AuNP and SF AgNP respectively, probably correspond with the O-H group (figure 9). Additionally, SAL AgNPs and SAL AuNPs also displayed respective visible bands at 1237.48 and 1257.18 cm-1 suggesting the stretching vibration of the C-O functional group. The weak but notable band at 1041.76 cm-1 for the SF AgNPs could be assigned as absorption bands for—C-O-C- whilst the 3238,56 cm-1 band may correspond to the N-H functional group. The bands corresponding to the C–O and O–H bonds on the FT-IR spectra indicate the possible involvement of phenolic acids, carbohydrates, flavonoids and terpenoids in the capping and stabilization of the synthesized nanoparticles [30, 40, 41]. The HPLC phytochemical profile of SAL has revealed that the plants' are high in flavonoid content especially rosmarinic and carnosic acid [12]. The involvement of compounds that contain hydroxyl and carbonyl groups in nanoparticle synthesis has been reported in numerous studies [30, 41, 42]. A study by Aboyade and colleagues reported that SF contained significant levels of free and protein-bound amino acids [17]. Balashanmugam and colleagues suggested that amino acids and proteins may act as stabilizers of nanoparticles after the bioreduction process [43]. The shifted band

Table 4. Comparison of FT-IR spectra of *S*AL and SF aqueous extracts and their respective nanoparticles.

	FT-IR peaks of aqueous extracts (cm^{-1})	FT-IR peaks of NPs (cm^{-1})	Shift value[a](cm^{-1})	Possible functional groups	References
SAL AgNP	3384.65	3414.29	−29.64	O-H (Alcohols)	9, 20, 40
	2927.83	2920.96	6.87	C-H (Alkanes)	9, 20, 32, 40, 41
	1609.34	1625.92	−16.58	C = C (Aromatics)	9, 30, 41
	1272.5	1237.48	35.02	C-O (Aromatic esters, Ethers, Carboxylic acids)	30, 41
SAL AuNP	3384.65	3405.97	21.32	O-H (Alcohols)	9, 20, 40
	2927.83	2907.03	20.8	C-H (Alkanes)	9, 20, 32, 40, 41
	1609.34	1618.43	−9.09	C = C (Aromatics)	9, 30, 41
	1272.5	1257.18	15.32	C-O (Aromatic esters, Ethers, Carboxylic acids)	30, 41
SF AgNP	3254.44	3238.56	15.88	N-H (Amine)	32
	2937.2	2911.52	25.68	C-H (Alkanes)	9, 20, 40
	1050.32	1041.76	8.56	C-O-C	30, 40, 41

[a]The shift values were calculated by subtracting the transmittance peak of synthesized NPs from the transmittance peak of the aqueous extracts.

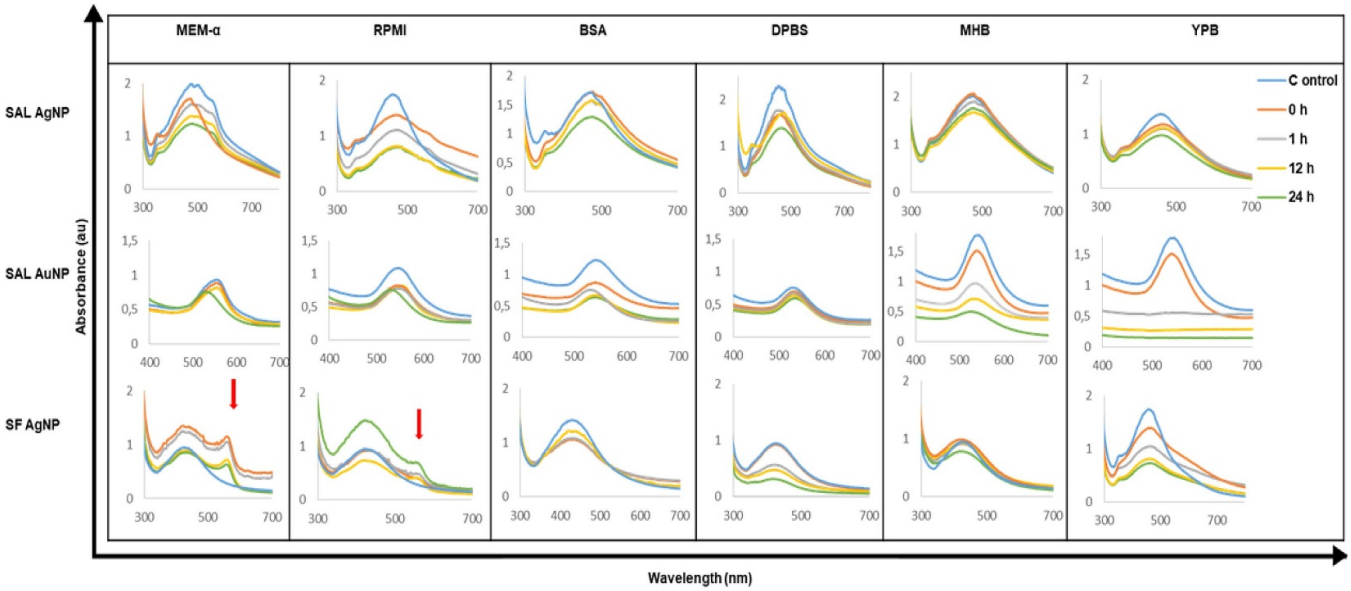

Figure 10. Stability of synthesised nanoparticles during incubation in biological media and buffers at 37 °C. UV–vis analysis of the AuNP and AgNP was perform over a 24 h period. Arrows show the peaks due to the phenol red content in the respective media. ***Abbreviations:*** BSA: Bovine Serum Albumin; DPBS: Dulbecco's Phosphate Buffered Saline; MEM-α: Minimum Essential Medium Eagle-Alpha Modification; MHB: Müeller Hinton Broth; RPMI: Roswell Park Memorial Institute medium.

at 3238.56 cm-1 in the FT-IR spectrum of SF AgNP, is attributed to the N-H group of amines, affirming the above suggestion. The benign nature of the identified capping and stabilizing agents may allow the use of the synthesized nanoparticles in the food, medicinal and cosmetic industries. However, further analysis of these synthesized nanoparticles is required for the precise identification of the actual molecules responsible for the synthesis of nanoparticles.

4.3.4. Stability of nanoparticles in biological media Any biomedical application of the nanoparticles would first require *in vitro* and *in vivo* testing. It is therefore important to confirm the stability of these nanoparticles in biological environments. Biologically stable nanoparticles do not aggregate when placed in biological media over an extended period of time [21]. The stability of the synthesized nanoparticles using SAL and SF extracts is reported in figure 10. Uv–vis analysis was used to determine changes in the stability of the nanoparticles. The stability of the nanoparticles was evaluated at 37 °C since most *in vitro* and *in vivo* applications are performed at this temperature. When the SAL AgNP and SF AgNP were placed to MHB, the absorption peaks changed only moderately, implying that the nanoparticles are stable in the respective media. However the absorption peaks of SAL AuNP flattened with time in both MHB and YPB, showing the

Table 5. The MIC values of SAL and SF extracts and synthesized nanoparticles against selected microorganisms.

Test samples (mg ml^{-1})	Bacterial strains *S. epidermidis*	*P. aeruginosa*
SAL extract	>50	>50
SAL AgNP	**0.1875****	**0.375****
SAL AuNP	–	–
SF extract	>50	>50
SF AgNP	**0.75****	**0.75****
Ampicillin	**0.001**	2

** Statistical significance ($p<0.001$) compared to the activity of synthesizing water extract. – means no activity observed with highest concentration of 1.5 mg ml^{-1}. MIC < 1 mg ml^{-1} are in bold.

unstable nature of the nanoparticles in the biological media. Even though the absorption spectra of the synthesized nanoparticles in the other biological media (MEM-α, RPMI, BSA, DPBS and YPB) broadened slightly over time, the resulting λ-max corresponding to the SPR of AgNP and AuNP did not change meaning synthesized SAL AgNP, SAL AuNP and SF AgNP were still present in solution. The broadening and slight flattening might be as a result of some of the synthesized nanoparticles disintegrating or agglomerating within the selected media [6]. Agglomeration has been reported to result in changes in the surface morphology of the synthesized nanoparticles [44]. A second red–shifted peak was observed for SF AgNPs in MEM-α and RPMI and shown by the red arrows in figure 8. This observation could be associated with the phenol content of the media. However, additional assays will be required for the confirmation of this assumption.

4.4. Antibacterial activity of SAL, SF and synthesized nanoparticles

This study found that water extracts of SAL and SF did not display any significant antibacterial activity against *S. epidermidis* and *P. aeruginosa*. This is in agreement with a previous study, which reported that water extracts of SF have only weak antimicrobial activity [13]. A natural agent is considered a noteworthy antimicrobial agent if it is MIC value is 1 mg ml^{-1} and below [45]. This study shows that both SAL AgNP and SF AgNP have MIC values below 1 mg ml^{-1}, which demonstrates that these NPs have significant antimicrobial properties. However, SAL AuNP did not have any antimicrobial properties, which suggest that the silver ions played a role in the antibacterial activity. A previous study investigated the antibacterial activity of colloidal AgNP that was produced by electrolysis and reported MIC values of 4 and 2 mg ml^{-1} for *S. epidermidis* and *P. aeruginosa*, respectively [46]. The antibacterial activity of both SAL AgNPs and SF AgNPs is thus significantly higher than colloidal AgNPs produced by electrolysis. It is likely that bioactive phytochemicals present in the plant extract were incorporated into the AgNPs, resulting in the production of biogenic AgNPs that have high antibacterial activity. However, further analysis which can identify the phytochemicals involved in the synthesis of SAL AgNPs and SF AgNPs is required. Other studies which describe the synthesis of biogenic AgNPs from plant extracts also reported the enhanced bioactivity of biogenic AgNPs when compared to the antibacterial activity of the plant extracts [6, 9, 47]. The difference in the antibacterial activity of SAL AgNPs and SF AgNPs could also result from the differences in the phytochemical composition of SAL and SF.

5. Conclusion

Since all plant species have a specific phytochemical blueprint, their potential to reduce metallic ions and produce nanoparticles is expected to be different. Additionally, the nanoparticles synthesized from different plants tend to display different characteristics as illustrated by our findings. SAL and SF water extracts were used to successfully produce Ag nanoparticles (SAL AgNPs and SF AgNPs, respectively). The SAL extract also produced Au nanoparticles (SAL AuNPs). The optimal plant extract concentrations to synthesize 1 mg ml^{-1} of SAL AgNPs, SF AgNPs and SAL AuNPs was 3.125, 6.25 and 3.125 mg ml^{-1} respectively. The optimal $AgNO_3$ and $NaAuCl_4 \cdot 2H_2O$ concentrations were 3 mM and 1 mM respectively. The optimal synthesis temperature was at 70 °C. HR-TEM confirmed the presence of spherical and polygon shaped biogenic nanoparticles of varying sizes. SAL AgNP and SF AgNP demonstrated significant antibacterial activity against *S. epidermidis* and *P. aeruginosa*. These two microorganisms are common causes of nosocomial infections. This suggest that these NPs may be useful agents to combat this form of infection.

These agents can eventually be incorporated into different products such as bandages and topical ointments for the treatment of open wounds prone to infections. It is therefore recommended that further investigations for clinical applications such as drug delivery and anticancer activities of these agents be assessed.

Author contributions:

Conceptualization, P. Dube, M. Meyer, and S. Meyer.; methodology, M. Meyer and P. Dube.; software, P. Dube.; validation, M. Meyer and A. Madiehe.; formal analysis, M. Meyer and A. Madiehe.; investigation, P. Dube.; resources, M. Meyer.; data curation, M .Meyer and P. Dube.; writing—original draft preparation, P. Dube.; writing—review and editing, M. Meyer, S. Meyer and A. Madiehe.; visualization, M. Meyer and A. Madiehe.; supervision, M. Meyer and S. Meyer.; project administration, M. Meyer.; funding acquisition, M. Meyer and S. Meyer. All authors have read and agreed to the published version of the manuscript."

Funding:

This research was funded by the South African National Research Foundation (Grant number: CSRP170525233248) and the DSI/Mintek Nanotechnology Innovation Centre (NIC).

Acknowledgments

P.D sincerely thanks the South African National Research Foundation for funding her scholarship. The authors thank Dr. Nicole Sibuyi and Dr. Abdulrahman M. Elbagory for their assistance.

Conflicts of interest:

The authors declare no conflict of interest. The funders had no role in the design of the study; in the collection, analyses, or interpretation of data; in the writing of the manuscript, or in the decision to publish the results.

ORCID iDs

Phumuzile Dube https://orcid.org/0000-0003-0540-4867
Samantha Meyer https://orcid.org/0000-0002-5167-0608
Abram Madiehe https://orcid.org/0000-0002-3935-467X
Mervin Meyer https://orcid.org/0000-0002-8296-4860

References

[1] Gudikandula K and Charya Maringanti S 2016 *J. Exp. Nanosci.* **11** 714–21
[2] Aromal S A and Philip D 2012 *Spectrochim. Acta.* A **97** 1–5
[3] Rajan R, Chandran K, Harper S L, Yun S I and Kalaichelvan P T 2015 *Ind. Crop. Prod.* **70** 356–73
[4] Parashar V, Parashar R, Sharma B and Pandey A C 2009 *Dig. J. Nanomater. Bios.* **4** 45-50
[5] Vijayan R, Joseph S and Mathew B 2018 *Artif. Cells. Nanomed. Biotechnol.* **46** 861–71
[6] Ahmed S, Saifullah Ahmad M, Swami B L and Ikram S 2016 *J. Radiat. Res. Appl. Sc.* **9** 1–7
[7] Elbagory A M, Cupido C N, Meyer M and Hussein A A 2016 *Molecules* **21** 1498
[8] Lukman A I, Gong B, Marjo C E, Roessner U and Harris A T 2011 *J. Colloid. Interface. Sci.* **353** 433–44
[9] Majoumouo M S, Sibuyi N R S, Tincho M B, Mbekou M, Boyom F F and Meyer M 2019 *Int. J. Nanomed.* **14** 9031
[10] Elbagory A M, Hussein A A and Meyer M 2019 *Int. J. Nanomed.* **14** 9007
[11] Kamatou G P, Van Vuuren S F, Van Heerden F R, Seaman T and Viljoen A M 2007 *S. Afr. J. Bot.* **73** 552–7
[12] Kamatou G P, Viljoen A M and Steenkamp P 2010 *Food. Chem.* **119** 684–8
[13] Katerere D R and Eloff J N 2005 *Phytother. Res.* **19** 779–81
[14] Van Wyk B E and Wink M 2004 *Medicinal plants of the world: An illustrated guide to important medicinal plants and their uses* (Portland: Timber Press)
[15] Ntuli S S, Gelderblom W C and Katerere D R 2018 *BMC Complement Altern. Med.* **18** 93
[16] Van Wyk B E and Albrecht C 2008 *J. Ethnopharmacol.* **119** 620–9
[17] Aboyade O M, Styger G, Gibson D and Hughes G 2014 *J. Altern. Complement. Med.* **20** 71–76
[18] Nielsen T R, Kuete V, Jäger A K, Meyer J J M and Lall N 2012 *BMC Complement Altern. Med.* **12** 74
[19] Kamatou G P P, Van Zyl R L, Van Vuuren S F, Figueiredo A C, Barroso J G, Pedro L G and Viljoen A M 2008 *S. Afr. J. Bot.* **72** 230–7
[20] Khan M, Khan M, Adil S F, Tahir M N, Tremel W, Alkhathlan H Z,, Al-Warthan A and Siddiqui M R H 2013 *Int. J. Nanomed.* **8** 1507
[21] Elbagory A M, Meyer M, Cupido C N and Hussein A A 2017 *Nanomaterials* **7** 417
[22] Balouiri M, Sadiki M and Ibnsouda S K 2016 *J. Pharm. Anal.* **6** 71–79
[23] Akhtar M S, Panwar J and Yun Y S 2013 *ACS Sustain. Chem. Eng.* **1** 591–602
[24] Benakashani F, Allafchian A R and Jalali S A H 2016 *Karbala Int. J. Mod. Sci.* **2** 251–8
[25] Obaid A Y, Al-Thabaiti S A, El-Mossalamy E H, Al-Harbi L M and Khan Z 2017 *Arab. J. Chem.* **10** 226–31
[26] Hoo C M, Starostin N, West P and Mecartney M L 2008 *J. Nanoparticle Res.* **10** 89–96
[27] Song J Y, Kwon E Y and Kim B S 2010 *Bioproc. Biosystems. Eng.* **33** 159
[28] Kasthuri J, Veerapandian S and Rajendiran N 2009 *Colloids. Surf.* B **68** 55–60
[29] MubarakAli D, Thajuddin N, Jeganathan K and Gunasekaran M 2011 *Colloids. Surf.* B **85** 360–5
[30] Philip D, Unni C, Aromal S A and Vidhu V K 2011 *Spectrochim. Acta.* A **78** 899–904
[31] Arunachalam K D, Annamalai S K and Hari S 2013 *Int. J. Nanomed.* **8** 1307
[32] Kumar B, Smita K, Cumbal L and Debut A 2014 *Saudi. J. Biol. Sci.* **21** 605–9
[33] Logeswari P, Silambarasan S and Abraham J 2015 *J. Saudi. Chem. Soc.* **19** 311–7
[34] Tripathy A, Raichur A M, Chandrasekaran N, Prathna T C and Mukherjee A 2010 *J. Nanopart. Res.* **12** 237–46
[35] Ibrahim H M 2015 *J. Radiat. Res. Appl. Sc.* **8** 265–75
[36] Song J Y and Kim B S 2009 *Bioproc. Biosystems. Eng.* **32** 79
[37] Ardani H K, Imawan C, Handayani W, Djuhana D, Harmoko A and Fauzia V 2017 *IOP Conf. Ser.: Mater. Sci. Eng.* **188** 012056
[38] Clogston J D and Patri A K 2011 *Zeta Potential Measurement* (Frederick: Human Press)
[39] Dipankar C and Murugan S 2012 *Colloids. Surf.* B **98** 112–9
[40] Kumar B, Smita K, Cumbal L and Debut A 2017 *Saudi. J. Biol. Sci.* **24** 45–50
[41] Philip D and Unni C 2011 *Physica.* E **43** 1318–22
[42] Yin X, Chen S and Wu A 2010 *Micro. Nano. Lett.* **5** 270–3
[43] Balashanmugam P, Durai P, Balakumaran M D and Kalaichelvan P T 2016 *J. Photoch. Photobio.* B **165** 163–73
[44] Zimbone M, Baeri P, Calcagno L, Musumeci P, Contino A, Barcellona M L and Bonaventura G 2014 *PloS One* **9** e89048
[45] Van Vuuren S F 2008 *J. Ethnopharmacol.* **119** 462–72
[46] Domínguez A V, Algaba R A, Canturri A M, Villodres Á R and Smani Y 2020 *Antibiotics* **9** 36
[47] Kathiravan V, Ravi S, Ashokkumar S, Velmurugan S, Elumalai K and Khatiwada C P 2015 *Spectrochim. Acta.* A **139** 200–5